

# RS-Prune: Training-Free Data Pruning at High Ratios for Efficient Remote Sensing Diffusion Foundation Models

Fan Wei<sup>1</sup> Runmin Dong<sup>2\*</sup> Yushan Lai<sup>4</sup> Yixiang Yang<sup>6</sup> Zhaoyang Luo<sup>4</sup>  
 Jinxiao Zhang<sup>1</sup> Miao Yang<sup>1</sup> Shuai Yuan<sup>5</sup> Jiyao Zhao<sup>3</sup> Bin Luo<sup>4</sup> Haohuan Fu<sup>1,3,4\*</sup>

<sup>1</sup>Department of Earth System Science, Tsinghua University

<sup>2</sup>School of Artificial Intelligence, Sun Yat-sen University

<sup>3</sup>National Supercomputing Center in Shenzhen

<sup>4</sup>Tsinghua Shenzhen International Graduate School, Tsinghua University

<sup>5</sup>Department of Geography, The University of Hong Kong

<sup>6</sup>Wangxuan Institute of Computer Technology, Peking University

## Abstract

Diffusion-based remote sensing (RS) generative foundation models are essential for various downstream tasks, such as super-resolution and image reconstruction. However, these models rely on large amounts of globally representative data, which often contain redundancy, noise, and class imbalance, reducing training efficiency and sometimes preventing convergence. Existing RS diffusion foundation models typically aggregate multiple classification datasets or apply simplistic deduplication, overlooking the distributional requirements of generation modeling and the inherent heterogeneity of RS imagery.

To address these limitations, we propose a training-free, two-stage data pruning approach that quickly selects a high-quality subset under high pruning ratios, enabling a preliminary foundation model to converge rapidly and serve as a versatile backbone for generation, downstream fine-tuning, and other applications. Our method jointly considers local information content with global scene-level diversity and representativeness. First, an entropy-based criterion efficiently removes low-information samples. Next, leveraging RS scene classification datasets as reference benchmarks, we perform scene-aware clustering with stratified sampling to improve clustering effectiveness while reducing computational costs on large-scale unlabeled data. Finally, by balancing cluster-level uniformity and sample representativeness, the method enables fine-grained selection under high pruning ratios while preserving overall diversity and representativeness. Experiments on both curated RS datasets and large-scale global imagery show that, even after pruning 85% of the training data, our method

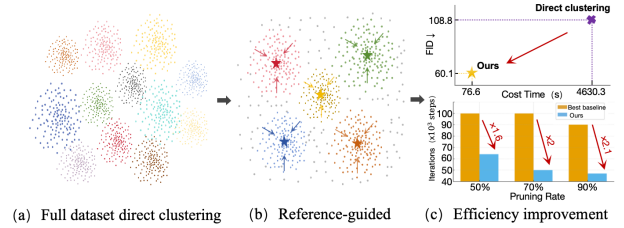


Figure 1. Illustration of our reference-guided clustering and efficiency gains. (a) Direct clustering on the full unlabeled dataset is computationally expensive. (b) Our reference-guided strategy selects a representative, scene-aware subset around reference centroids. (c) Compared with full-dataset clustering, our method achieves much lower FID at substantially reduced cost time. And compared with best baseline, ours requires 1.9x to 2.1x fewer training iterations across different pruning ratios.

significantly improves convergence and generation quality. Furthermore, diffusion foundation models trained with our method consistently achieve state-of-the-art performance across downstream tasks, including super-resolution and semantic image synthesis. This data pruning paradigm offers practical guidance and empirical insight for the development of RS generative foundation models.

## 1. Introduction

In recent years, generation models, especially diffusion models [13, 25], have achieved remarkable progress in fields such as computer vision [27], medical imaging [35], and remote sensing (RS) [9]. Within the RS domain, generation models have been widely applied to data augmentation, image reconstruction, super-resolution, and high-resolution image synthesis, supporting practical applica-

\*Corresponding authors.

tions in urban planning, land-use monitoring, and disaster response [4]. A powerful RS diffusion foundation model can provide a robust data and modeling backbone to further enhance these applications.

However, the effective training of RS diffusion foundation models critically depends on the quality and distribution of training data. The emergence of large-scale open-source datasets (e.g., Git-10M [20], RS5M [51]) provides valuable resources, yet it also introduces several critical challenges, including image redundancy, low-quality samples (e.g., noise and cloud cover), class imbalance [7], and scene homogeneity [40]. These issues not only hinder the training efficiency of RS foundation models but also limit the effectiveness of the resulting pretrained models on downstream tasks.

Recently, several studies in RS generation tasks have made preliminary explorations into data processing. For instance, RSDiff employs size cropping and noise augmentation [33]. WHU-RS19 [2] removes cloud and open-ocean regions to reduce low information content. Super-resolution works [15] often prioritize urban areas. Nevertheless, these methods mainly rely on rule-based or simplistic strategies to eliminate redundant data, without considering the specific dependence of generation models on data distribution [11] or the inherent characteristics of RS imagery, such as diversity, heterogeneity, and class balance. Moreover, many data pruning methods developed in the computer vision domain rely on scoring mechanisms [45] from supervised pre-trained models [26] or retrieval of nearby images based on ImageNet benchmarks [24]. In contrast, a standardized labeled dataset for RS, comparable to ImageNet [8] in computer vision and spanning multiple resolutions and modalities, is currently lacking. Overall, systematic research on data selection for RS diffusion foundation models remains scarce.

The effectiveness of diffusion foundation models depends more on the quality and distribution of the training data than on dataset size alone. Recent studies [6] have shown that diffusion models retain strong generation performance even when a large fraction (e.g., 90% of ImageNet samples) of the training data is removed, highlighting that a significant portion of the data contributes minimally. In the RS domain, raw data often contains substantial redundancy and noise, meaning that merely increasing the dataset size does not guarantee proportional performance gains. If generative models are trained on large volumes of data without appropriate selection, low-quality and redundant samples can not only slow convergence and increase computational and time costs, but also introduce distribution shifts that ultimately degrade model performance.

To address these issues, we propose an efficient, training-free data pruning approach for RS generative diffusion models, which can construct a diverse subset under

high pruning ratios, enabling diffusion models to converge significantly faster with better generative quality.

More specifically, targeting redundancy, low quality samples, and class imbalance, we systematically explore data pruning strategies across both global-scale scenarios (GiT-10M, RS5M) and urban-scale settings (our constructed USA-1m multispectral dataset). The method proceeds along two complementary dimensions: 1) Information dimension. We employ entropy-based pruning to rapidly discard low texture or homogeneous large-area regions, thereby reducing redundancy and compressing subsequent computation costs. 2) Diversity and representativeness dimension. We introduce scene-aware clustering with stratified sampling. Using existing RS scene-classified datasets as reference, we perform over-clustering on the reference datasets to obtain hundreds of cluster centroids, effectively avoiding the high computational cost of full-scale clustering and full dataset training. Large-scale unlabeled datasets are then assigned to these predefined clusters in the clustering space. Samples are subsequently selected using a combination of class-balanced allocation and centroid-prioritized sampling, which preferentially chooses samples near cluster centers to preserve scene-representative characteristics while maintaining diversity.

Extensive experiments reveal three key observations: First, both datasets specifically constructed for RS generation models and globally collected datasets contain substantial redundancy, and appropriate data pruning accelerates convergence while yielding models that outperform those trained on the full datasets. Second, entropy-based pruning consistently removes low quality and highly homogeneous samples, providing stable improvements across varying pruning rates. Third, optimal pruned subsets are obtained by combining entropy-based filtering with strategies that preserve diversity and representativeness at the scene level, ensuring that informative and representative samples are retained for effective model training.

Our main contributions in this paper can be summarized as follows:

- We systematically explore data pruning for RS diffusion foundation models and propose a training-free, two-stage selection strategy that considers data heterogeneity, diversity, and representativeness, enabling faster convergence and improved generation performance under high pruning ratios.
- We introduce a reference-guided clustering method, performing pre-clustering on curated scene-classified datasets to preserve the diversity of scene cluster centers while avoiding the computational cost of clustering massive unlabeled datasets and full-dataset training.
- Extensive experiments demonstrate that our method can rapidly construct a high-quality training subset with substantial scale reduction. Training on this subset not only

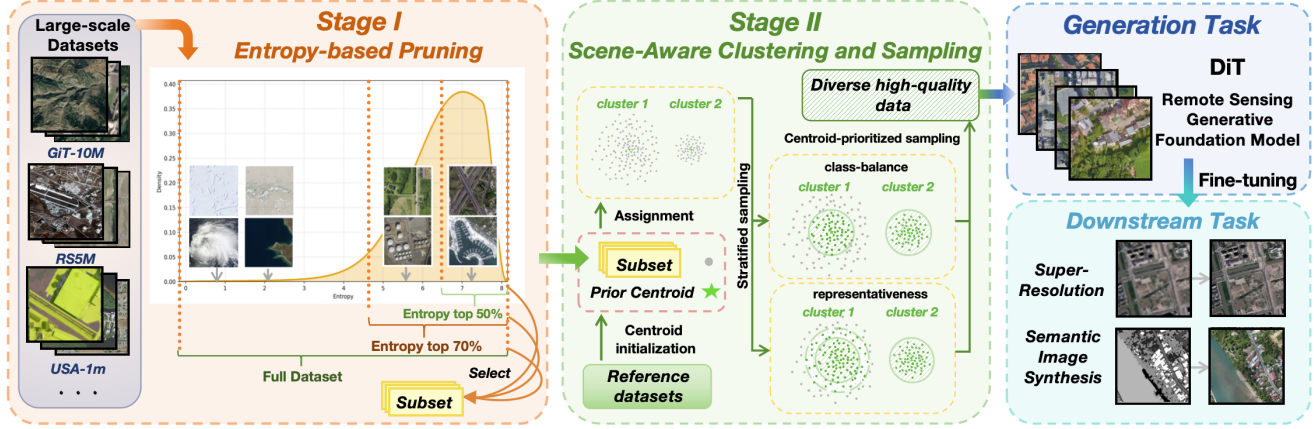


Figure 2. Overview of our multi-stage data pruning method for Remote Sensing generative foundation models.

accelerates model convergence significantly but also outperforms prior state-of-the-art methods in pre-training generation quality while achieving gains on downstream tasks.

## 2. Related Work

### 2.1. Diffusion foundation Models

Diffusion foundation models [32] play a pivotal role in image generation, data synthesis, and image reconstruction. For instance, Stable Diffusion (SD) 1.5 [29] leverages latent-space representations together with a UNet backbone, serving as a lightweight generation foundation model that provides strong pretrained initialization for ControlNet [47] and related low-level vision tasks [30]. More recently, Transformer-based architectures such as DiT [25] have emerged, while models like SD3 [10] and Flux [3] offer substantially stronger generation capabilities and higher fidelity, further advancing the scalability and versatility of diffusion frameworks.

In the RS domain, diffusion foundation models have also started to gain attention. To address the unique properties of RS imagery, such as multi-spectral and multi-resolution observations, geospatial information, and global coverage, many works have explored pre-training or fine-tuning foundation models on RS datasets [38, 39, 43]. For example, DiffusionSat [16] introduced geolocation as conditioning information and fine-tuned Stable Diffusion 1.5 on multi-source RS data, supporting multiple RS generation tasks. Meanwhile, models such as SR3 [31] and CDM [14], demonstrated strong super-resolution performance on natural images, providing a foundation for their adaptation to RS. Despite these advances, existing RS generation models typically aggregate multiple classification datasets or apply simplistic deduplication [22], thereby overlooking the distributional requirements of generation foundation modeling

as well as the inherent heterogeneity and diversity of RS imagery. Consequently, the field lacks systematic exploration of data pruning strategies specifically designed to address the characteristics of remote sensing data and the requirements of RS generative foundation models.

### 2.2. Data Pruning Methods

Training data are critical to constructing RS diffusion foundation models. However, existing studies [21, 33] in this field have adopted simplistic deduplication and preprocessing strategies, such as removing cloud and ocean regions [2] and prioritizing urban areas [48]. These approaches are insufficient to address the sensitivity of generation models to data distribution, heterogeneity, and class imbalance.

Current data pruning methods can be broadly categorized into three types. First, data-valuation methods assign an importance score to each sample and select samples accordingly. For example, MoSo [37] estimates the change in empirical risk when a sample is removed. Although such methods are generally efficient, their performance can be affected by group effects and may lack generalization in complex real-world settings. Second, distribution-based methods rely on the geometric structure of the dataset. For instance, Moderate-DS [42] selected samples near the median. CCS [52] balanced data distribution and sample importance during selection. Finally, optimization-based methods leverage optimization techniques to guide sample pruning, such as temporal dual-depth scoring [50], gradient matching [17], scalable self-supervised pruning metrics [36], influence functions [18], and bilevel optimization [5].

Most of these approaches are designed for supervised datasets and rely on scores generated by pre-trained supervised models. In practice, they typically require training or computation over the full dataset, which requires labeled data and is computationally expensive, making them diffi-

cult to scale to large, mostly unlabeled RS datasets.

Beyond explicit pruning algorithms, recent foundation models have also explored large-scale data pruning pipelines. For example, DINOv2 [24] constructs its curated LVD-142M dataset by performing PCA-hash and copy-detection based deduplication, followed by self-supervised retrieval based on ImageNet benchmarks. Similarly, V-JEPA 2 [1] adopts a retrieval and reweighting strategy to align large-scale video data with target distributions.

However, such data curation pipelines typically rely on target datasets or distributions and require large-scale clustering or retrieval over the entire datasets. In remote sensing, there is no benchmark similar to ImageNet that adequately captures the diversity of global RS imagery, and RS diffusion foundation models are particularly sensitive to the diversity and representativeness of semantic categories. To bridge this gap, we systematically explore training-free, unsupervised data pruning strategies tailored to the characteristics of RS imagery and the requirements of RS diffusion foundation models.

### 3. METHOD

#### 3.1. Workflow

RS generative foundation models depend on large-scale, globally collected datasets that provide high quality, diversity, and representativeness. However, existing RS datasets often lack these characteristics, leading to slower model convergence, suboptimal generation performance, and insufficient capability to support various low-level downstream tasks. To address this, we propose a two-stage data pruning method (Fig. 2) guided by two key principles:

**1) Informational value** Cloud-covered or excessively homogeneous RS images are inevitable in global data collection. Such images are typically low-quality, contain limited informative content, and exhibit substantial redundancy. Images with higher information content, capturing meaningful structures and fine details, are prioritized for selection. This process effectively removes low-information and trivially homogeneous scenes, such as vast desert expanses, thereby preserving heterogeneity in the selected subset.

**2) Scene diversity and centroid representativeness** While maintaining the overall semantic distribution, rare scenes are preferentially preserved. For scenes with abundant samples, candidates are ranked by their similarity to the cluster centroid, and the nearest-centroid samples are selected. This strategy not only ensures high quality and de-redundancy but also aligns with expert priors reflected in reference datasets, producing a subset that is both distributionally representative and diverse.

#### 3.2. Stage I: Entropy-based Pruning

We measure the information value of each image by computing its global Shannon entropy [34]. Specifically, for an image  $I$ , we compute its grayscale entropy  $H(I)$  to capture the diversity of pixel intensities:

$$H(I) = - \sum_{k=0}^{L-1} p_k \log p_k, \quad (1)$$

where  $p_k$  denotes the empirical probability of intensity level  $k$  among  $L$  possible levels. Images with  $H(I) < \tau$  are discarded, as they typically correspond to invalid regions (e.g., sensor noise) or low-variation scenes (e.g., clouds, open ocean, deserts, or saturated exposures). This pruning step substantially reduces dataset size while preserving high-information candidate samples.

#### 3.3. Stage II: Scene-Aware Clustering and Sampling

The remote sensing domain lacks a universally adopted, comprehensive benchmark comparable to ImageNet in the natural image domain. To address this, we leverage multiple expert-curated RS classification datasets as a composable bank of clustering priors, covering various scene types such as urban areas, cropland, water bodies, forests, and transportation infrastructure. Unlike approaches that apply label-free clustering and sampling directly on a massive generic corpus, we first establish stable scene centroids on this prior bank. Importantly, instead of computing centroids separately for each labeled category, we conduct over-clustering across the entire prior dataset to obtain diverse and representative centroids. Subsequently, for the large-scale unlabeled RS dataset, samples are aligned to these centroids and selected according to centroid-prioritized sampling, ensuring both representativeness and diversity. This pipeline uses expert-curated classification datasets to derive more representative cluster centroids, thereby enhancing diversity and representativeness in the selected subset, while simultaneously reducing the computational cost of clustering the full unlabeled large-scale dataset.

**Prior Centroid Construction.** We employ a unified feature extractor  $f(\cdot)$ , namely Git-RSCLIP [20], with  $\ell_2$  normalization to embed all images from standard datasets. Git-RSCLIP is specifically pretrained on large-scale remote sensing corpora and achieves substantially better performance than previous RS-oriented CLIP variants such as RemoteCLIP and GeoRSCLIP.

$$\mathbf{z}_x = \frac{f(x)}{\|f(x)\|_2} \quad \text{for each } x \in \mathcal{D}_{\text{ref}}, \quad (2)$$

where  $\mathcal{D}_{\text{ref}}$  is the collection of reference (prior) datasets.  $x$  is an image sample of the datasets.  $f(\cdot)$  is a pretrained image encoder.  $\mathbf{z}_x$  is the  $\ell_2$ -normalized embedding of  $x$ . We

then perform  $K$ -means clustering on the unit hypersphere to identify representative scene centroids. Let  $\mathcal{M}$  denote the set of learned centroids:

$$\mathcal{M} = \{\boldsymbol{\mu}_k\}_{k=1}^K, \quad \|\boldsymbol{\mu}_k\|_2 = 1, \quad (3)$$

where  $K$  is the number of clusters and  $\boldsymbol{\mu}_k$  is the  $k$ -th centroid in the feature space.

**Cluster Assignment and Candidate Pooling.** For each unlabeled sample  $x \in \mathcal{D}_u$ , we compute its cosine similarity to all prior centroids:

$$s_k(x) = \langle f(x), \boldsymbol{\mu}_k \rangle, \quad k = 1, \dots, K, \quad (4)$$

where  $s_k(x)$  is the similarity score.  $f(x)$  denotes the feature embedding of  $x$ . Each sample is assigned to the cluster with the highest similarity:

$$\hat{z}(x) = \arg \max_k s_k(x), \quad (5)$$

where  $\hat{z}(x)$  is the hard cluster label. The sample is then added into the candidate pool corresponding to its assigned cluster, denoted  $P_k$ . This assignment procedure scales linearly with both the number of unlabeled samples and the number of centroids, making it efficient for large-scale datasets.

**Cluster-Aware Stratified Sampling.** Given a total sampling budget  $B$ , we combine class-balanced allocation with centroid-prioritized sampling.

- **Class-balanced allocation.** Let  $\{P_k\}_{k=1}^K$  denote the candidate pools for  $K$  clusters, and let  $q = \lfloor B/K \rfloor$ . We assign each cluster a quota of  $q$  samples to ensure coverage across clusters. Rare clusters with fewer than  $q$  samples retain all candidates, preserving diversity.
- **Centroid-prioritized sampling.** Within each cluster  $k$ , we rank samples  $x \in P_k$  by their similarity  $s_k(x)$  to the cluster centroid  $\boldsymbol{\mu}_k$  and select the top- $q$  samples:

$$S_k = \text{Top-}q_{x \in P_k} s_k(x). \quad (6)$$

If  $|P_k| < q$ , we set  $S_k = P_k$  and reallocate the remaining budget by selecting additional samples from the global remainder:  $P_{\text{rem}} = \bigcup_{j=1}^K (P_j \setminus S_j)$  in descending order of similarity until the total number of selected samples equals  $B$ , i.e.,  $B = \sum_{k=1}^K |S_k|$ .

### 3.4. Complexity Analysis

In stage I, the overall complexity is approximately  $\mathcal{O}(N)$ , as each image is evaluated individually for information value.

In stage II, we have: 1) Building clustering priors on a small standardized reference set is done once, so its cost is negligible relative to the full pipeline. 2) Assigning each

image to the most similar centroid requires computing similarities to  $K$  centroids in a  $f_d$ -dimensional feature space, giving  $\mathcal{O}(NKf_d)$ . 3) Within each cluster, ranking images by similarity and sampling  $q$  samples requires sorting, which has a complexity of  $\mathcal{O}\left(\frac{N}{K} \log \frac{N}{K}\right)$  per cluster, resulting in  $\mathcal{O}(N \log \frac{N}{K})$ . Since  $K$  and  $f_d$  are small constants in practice, the end-to-end complexity can be considered  $\mathcal{O}(N \log N)$ . The method does not involve training deep models. The core operations are vector arithmetic, similarity computation, and sorting. Consequently, the pipeline is highly scalable and practically deployable for data pruning over large-scale RS datasets.

## 4. EXPERIMENTS

### 4.1. Datasets and evaluation

To evaluate the effectiveness of our data pruning approach for RS generation tasks, we conduct experiments on both global-scale and urban-scale datasets. Specifically, we use two representative global-scale optical datasets (i.e., GIT-10M and RS5M) that were carefully curated for RS generative foundation models, as well as a large-scale urban-scale multispectral dataset (i.e., USA-1m) collected in this work based on U.S. urban boundary products [19]. The global datasets provide broad coverage and diversity, while the urban dataset offers finer spatial resolution and richer texture information. This design allows us to assess the effectiveness and generalizability of our data pruning strategy across datasets with varying resolutions, modalities, volumes, and sensors.

- **Git-10M** [20] A *global-scale* dataset comprising 10.5M satellite images (RGB) with a spatial resolution of 0.5 to 128 m, which spans multiple continents and geographic regions, covering diverse land-cover types such as urban areas, croplands, forests, mountains, and deserts.
- **RS5M** [51] A *global-scale* dataset initially collected from 11 publicly available image–text pair datasets, containing RS images (RGB) from different regions, resolutions, and scene types. Due to large variations in image size and relatively low data quality, we apply simple preprocessing and filtering, resulting in a curated subset of about 1.04M images.
- **USA-1m (multispectral)** Our self-constructed, urban-scale remote sensing dataset consisting of 8.77M four-channel, high-resolution (1 m) images, derived from the USDA National Agriculture Imagery Program (NAIP) [28]. The dataset covers major urban areas across 45 U.S. states, with a total footprint of  $1.34339 \times 10^6 \text{ km}^2$ .

For each of the aforementioned datasets, we selected 5,000 high-quality images for subsequent metric computation for the generation task.

In Stage II, we adopt five scene-classification datasets

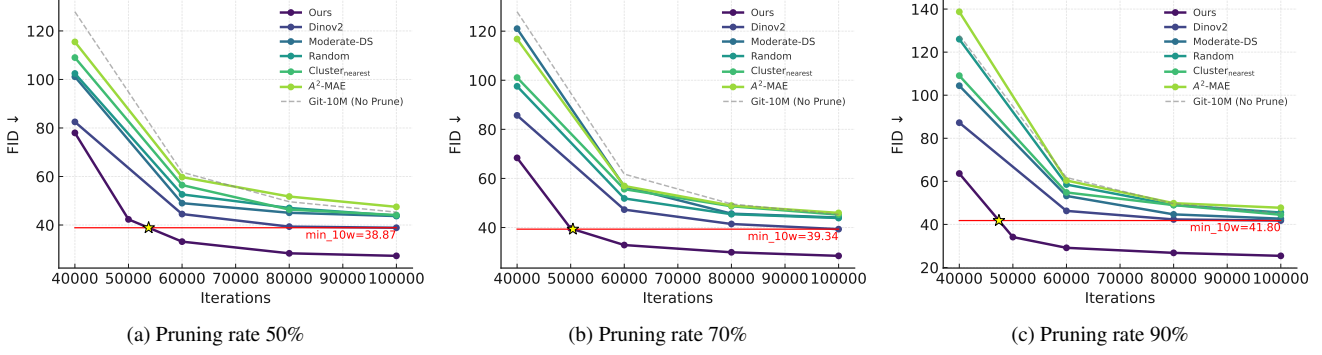


Figure 3. Comparison of generation performance (FID) across different pruning ratios on Git-10M.

Table 1. Experimental results with different data pruning methods on Git-10M and USA-1m. We report results at a pruning ratio of 70%.

Method	Git-10M					USA-1m						
	Generation		SR		SIS		Generation		SR		SIS	
	FID↓	FID↓	LPIPS↓	FID↓	LPIPS↓	FID↓	FID↓	LPIPS↓	FID↓	LPIPS↓	FID↓	LPIPS↓
Full Dataset	45.30	89.25	0.3912	125.79	0.6027	242.52	125.90	0.4909	327.33	0.8212		
Random	43.87	89.25	0.3912	127.00	0.6200	255.11	126.63	0.4827	236.68	0.6698		
Moderate-DS [42]	44.07	92.40	0.3952	132.85	0.6222	199.24	124.86	0.5098	233.13	0.6730		
Cluster <sub>nearest</sub> [6]	45.24	89.58	0.3898	133.18	0.6237	201.36	150.11	0.5870	256.40	0.6804		
Dinov2 [24]	39.34	91.76	0.3930	137.55	0.6121	180.98	127.73	0.5472	238.80	0.6761		
A <sup>2</sup> -MAE [48]	45.96	90.39	0.3938	130.64	0.6013	360.74	148.36	0.6028	256.39	0.6993		
<b>Ours</b>	<b>28.46</b>	<b>87.98</b>	<b>0.3893</b>	<b>122.08</b>	<b>0.5967</b>	<b>175.93</b>	<b>122.00</b>	<b>0.4779</b>	<b>199.82</b>	<b>0.6682</b>		

with distinct characteristics: NWPU-RESISC45 [7], UC Merced Land-Use [46], AID [40], WHU-RS19 [2], and RSD46-WHU [23]. Detailed information regarding their resolution, dataset size, number of classes, and data sources can be found in supplementary materials.

To comprehensively assess the impact of training data on RS generation models, we evaluate their generation capability directly on the test set and further use downstream-task metrics to evaluate the capability of the pretrained models, i.e., super-resolution (SR) and semantic image synthesis (SIS). The evaluation metrics include FID [12] and LPIPS [49]. Lower LPIPS and FID values indicate superior generation performance.

- **SECOND-SR** We construct a super-resolution dataset based on the high-resolution SECOND semantic change detection benchmark [44]. Low-resolution (LR) images are generated by first downsampling and then upsampling the original high-resolution (HR) images. The dataset contains 4,662 paired LR–HR images, each with a spatial size of 512×512 pixels, covering six major land-cover classes.
- **OpenEarthMap** [41] A global benchmark designed for semantic segmentation. It consists of 5,000 RS images across six continents at 0.25 to 0.5 m resolutions. Labels are annotated with eight land-cover categories.

## 4.2. Implementation Details

All models are implemented using the official DiT framework [25], which is a transformer-based architecture using its github repository<sup>1</sup>. We adopt the DiT-XL/2 backbone for both generation pretraining and downstream tasks. All experiments are conducted with 256×256 input size, a global batch size of 256, and AdamW optimizer with a fixed learning rate of  $1 \times 10^{-4}$ .

Training is distributed across 4 NVIDIA H100 GPUs.

**Base VAE** For Git-10M and RS5M, we use the publicly released Stable Diffusion VAE (sd-vae-ft-ema)<sup>2</sup>. For USA-1M, we train a custom four-channel VAE from scratch and select the checkpoint with the lowest validation loss.

**Generation pretraining** DiT is trained in an unconditional setting. For each dataset, we run 40K to 100K diffusion steps and models are trained from scratch. **Downstream fine-tuning** For super-resolution and semantic image synthesis, we initialize from the pretrained DiT checkpoints and fine-tune for 5,000 steps per task.

## 4.3. Comparison Results

We compare the proposed method with three groups of pruning strategies: basic pruning methods (e.g., Random, Moderate-DS [42]), data pruning methods for founda-

<sup>1</sup><https://github.com/facebookresearch/DiT>

<sup>2</sup><https://huggingface.co/stabilityai/sd-vae-ft-ema>

Table 2. Results of scene-aware clustering and sampling at high pruning ratios. The subset refers to the Stage I output used as input for Stage II.

Pruning ratio	Subset	Stage I	Stage II	Git-10M			RS5M		
				generation FID $\downarrow$	SIS FID $\downarrow$	LPIPS $\downarrow$	generation FID $\downarrow$	SIS FID $\downarrow$	LPIPS $\downarrow$
85%	$D_{15\%}^{H\uparrow}$	✓		68.7814	125.7938	0.6044	59.4955	126.7798	0.5966
	$D_{30\%}^{H\uparrow}$	✓	✓	<b>61.3269</b>	<b>120.5167</b>	<b>0.5982</b>	<b>58.9813</b>	<b>115.6430</b>	<b>0.5902</b>
	$D_{50\%}^{H\uparrow}$	✓	✓	64.4233	139.9440	0.6139	73.7312	132.6490	0.6014
	$D_{70\%}^{H\uparrow}$	✓	✓	72.3580	130.6310	0.6139	75.4898	121.8777	0.5941
90%	$D_{10\%}^{H\uparrow}$	✓		70.9027	121.9285	0.6043	65.4067	124.6616	0.6034
	$D_{30\%}^{H\uparrow}$	✓	✓	63.6400	123.0029	0.6106	64.2536	124.8206	0.6004
	$D_{50\%}^{H\uparrow}$	✓	✓	64.2870	144.4404	0.6173	71.3744	130.5425	0.6094
	$D_{70\%}^{H\uparrow}$	✓	✓	77.2366	131.4739	0.6094	79.8913	128.3239	0.5970

tion models (e.g., Dinov2 [24], A<sup>2</sup>-MAE [48]), and a recent approach specifically developed for generation models (Cluster<sub>nearest</sub> [6]). To examine their effectiveness across varying scene complexities, experiments are conducted on a global-scale dataset (Git-10M) and an urban-scale dataset (USA-1m). To ensure comparability, all models are trained for an equivalent number of iterations, 100K for Git-10M and 40K for USA-1m, and the best results during training are reported. Beyond generation evaluation on the test set, pretrained models are further assessed on two downstream tasks, i.e., SR and SIS, with the top fine-tuning results recorded.

In subsequent experiments, we observe that the evaluation metrics on the generative task exhibit consistent trends with the evaluation metrics on different downstream tasks. This suggests that generative metrics can effectively characterize the capability of the pretrained models. Therefore, in some experiments, we use the generative metrics as a representative metrics for assessing pretrained model capacity.

As illustrated in Fig. 3, using Git-10M as an example, our method converges faster than the comparison methods across different pruning ratios. At different training steps, our method consistently achieves substantially lower FID than all competing approaches. With only about 50k training steps, our FID approaches the best scores of competitors at 100K.

Tab. 1 presents results at a fixed pruning ratio of 70% on both datasets. The proposed method achieves the best performance across generation and downstream tasks, demonstrating strong robustness and generalization. In addition, A<sup>2</sup>-MAE, designed for global-scale datasets, exhibits a notable performance drop on the urban-scale USA-1m. On Git-10M, our method achieves the lowest generation FID (28.45), representing a 27.7% improvement over the next best score (39.34). It further improves performance on super-resolution and semantic image synthesis, demonstrating strong alignment between downstream metrics and gen-

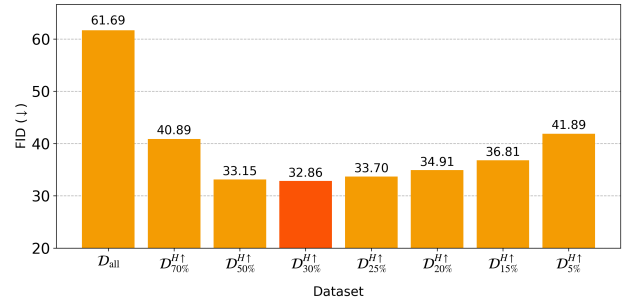


Figure 4. Results of entropy-based pruning at different pruning ratios on GiT-10M, reporting FID for the generation task.

Table 3. Results of stage I+II method at different pruning ratios.

Pruning ratio	Git-10M			RS5M		
	Generation FID $\downarrow$	SIS FID $\downarrow$	LPIPS $\downarrow$	Generation FID $\downarrow$	SIS FID $\downarrow$	LPIPS $\downarrow$
0%	127.8932	143.2622	0.6236	113.3864	137.9567	0.6076
30%	100.3227	134.2329	0.6064	81.9246	122.9466	0.5950
50%	84.3062	134.8372	0.6172	80.7609	121.7632	0.6002
70%	70.0361	131.7129	0.6045	63.3343	125.0599	0.5950
85%	<b>61.3269</b>	<b>120.5167</b>	<b>0.5982</b>	<b>58.9813</b>	<b>115.6430</b>	<b>0.5902</b>
90%	63.6400	123.0029	0.6106	64.2536	124.8206	0.6004

eration FID. On USA-1m, our approach also achieves consistent improvements across metrics, further confirming its effectiveness and generalizability to multispectral remote sensing imagery. More in-depth analyses regarding training steps are provided in supplementary materials.

#### 4.4. Ablation Study

##### 4.4.1. Effectiveness of entropy-based pruning

To validate the effectiveness of entropy-based pruning, we conduct experiments on the Git-10M dataset. Images are ranked in descending order of Shannon entropy, and the top

Table 4. Generative quality and runtime of clustering on full unlabeled data, entropy-pruned unlabeled data and our reference dataset-guided approaches.

Method	Cluster sample size	Cluster Numbers	Feature Dimension	Times(s)	FID $\downarrow$
Full unlabeled clustering	10.5 million	200	1024	4630.3	108.84
Entropy-pruned unlabeled clustering	3.1 million	200	128	308.4	71.16
Reference-guided (single, 21 classes)	2,100	200	1024	82.3	61.69
Reference-guided (single, 45 classes)	31,500	200	1024	<b>76.6</b>	<b>60.14</b>
Reference-guided (3 datasets)	43,600	200	1024	101.8	62.28
Reference-guided (5 datasets)	55,605	200	1024	115.1	60.65

$p\%$  subset is retained, denoted as  $\mathcal{D}_{p\%}^{H\uparrow}$ , while the unfiltered dataset is denoted as  $\mathcal{D}_{\text{all}}$ . Under a fixed training budget of 60K iterations, generation models trained on each subset are evaluated using FID, as shown in Fig. 4. On this global-scale dataset, retaining only the top 30% of images achieves the best FID (32.86), substantially outperforming the full dataset (61.69), highlighting the importance of removing low-information data. We further observe that as the pruning threshold becomes more stringent, FID initially decreases and then increases, indicating that the optimal pruning ratio should be chosen based on the redundancy level of the dataset. Analyses of different datasets and optimal pruning ratios are provided in supplementary materials.

#### 4.4.2. Effectiveness of scene-aware clustering and sampling

In this section, we conduct experiments on two datasets with different scales, including GiT-10M (tens of millions) and RS5M (millions), to evaluate the effectiveness of stage II, as shown in Tab. 2. On GiT-10M, pruning at 85% and 90% leads stage II to outperform stage I alone by approximately 10%. Similarly, on RS5M, stage II delivers notable benefits under high pruning, with corresponding improvements in downstream SIS performance. This is because, under high pruning ratios, stage I sampling alone leads to insufficient sample representativeness, and clustering is required to preserve diversity and distributional coverage. Overall, stage II consistently provides stable gains across both large- and medium-scale datasets, with especially pronounced advantages in highly compressed scenarios. And additional ablations on sampling strategies in stage II can be found in supplementary materials.

Tab. 3 further analyzes our two-stage method (stage I + stage II) under different pruning ratios. On both GiT-10M and RS5M, model performance steadily improves as the pruning ratio increases, with the best generative quality and downstream task results achieved at around 85% pruning. When the pruning ratio reaches 90%, the metrics exhibit a slight degradation, yet they remain clearly superior to training on the full unpruned dataset. These results indicate

that our approach enables the training of strong pretrained models even after discarding the vast majority of training samples, and that its effectiveness is robust and transferable across both large- and medium-scale remote sensing datasets.

#### 4.4.3. Effectiveness of reference dataset-guided clustering method

We further perform ablation studies on the proposed reference-guided clustering strategy in comparison with the standard practice of clustering directly on the unlabeled dataset. As reported in Tab. 4, our approach consistently surpasses clustering the full unlabeled collection in both runtime efficiency and generative quality. Even the widely adopted MiniBatch KMeans variant, which reduces the feature dimensionality from 1024 to 128 with subsequent normalization, remains less effective. The improvement arises from exploiting expert-curated reference datasets to derive more representative scene prototypes, thereby facilitating faster sample assignment and enhancing FID.

We also examine the influence of reference dataset selection, varying in scene diversity and dataset scale, together with the associated degree of over-clustering. Experiments conducted with datasets of different complexity levels and their combinations yield several observations. An important finding is that the diversity of scene categories in the reference dataset plays a critical role, as datasets with broader coverage produce more representative clustering outcomes. Another key observation is that the number of clusters  $K$  admits a moderate optimal range, with  $K=200$  emerging as a robust configuration that adequately covers common RS scenes while avoiding the breakdown of scene-balanced sampling caused by excessive fragmentation. Finally, we note that a simple aggregation of multiple scene classification datasets is not automatically beneficial, since distributional discrepancies across datasets may impede the alignment of semantically related categories and thus undermine representativeness. Therefore, effective dataset integration requires consideration of both scene complementarity and domain compatibility. Due to the limited space, limitation

and future work can be seen in supplementary materials.

## 5. CONCLUSION

In this work, we comprehensively explore data pruning for RS generative foundation models across datasets of varying scale and coverage. We propose a training-free, two-stage pruning strategy that jointly accounts for data heterogeneity, diversity, and representativeness. By avoiding the computational of large-scale clustering and model training, our approach enables rapid pruning of massive datasets into a high-quality subset under high pruning ratios, thereby accelerating the convergence of remote sensing generative foundation models and providing a strong data and modeling backbone for subsequent downstream applications. Our approach offers practical guidance and empirical findings that support the development of future remote sensing generative foundation models.

## References

- [1] Mido Assran, Adrien Bardes, David Fan, Quentin Garrido, Russell Howes, Mojtaba, Komeili, Matthew Muckley, Ammar Rizvi, Claire Roberts, Koustuv Sinha, Artem Zholus, Sergio Arnaud, Abha Gejji, Ada Martin, Francois Robert Hogan, Daniel Dugas, Piotr Bojanowski, Vasil Khalidov, Patrick Labatut, Francisco Massa, Marc Szafraniec, Kapil Krishnakumar, Yong Li, Xiaodong Ma, Sarath Chandar, Franziska Meier, Yann LeCun, Michael Rabbat, and Nicolas Ballas. V-jepa 2: Self-supervised video models enable understanding, prediction and planning, 2025. [4](#)
- [2] M. Balestra, M. Paolanti, and R. Pierdicca. WHU-RS19 ABZSL: An attribute-based dataset for remote sensing image understanding. *Remote Sensing*, 17(14):2384, 2025. [2](#), [3](#), [6](#)
- [3] Black Forest Labs. Flux.1: Official inference repository, 2024. [3](#)
- [4] S. Borana and S. Yadav. Urban land-use susceptibility and sustainability—case study. In *Water, Land, and Forest Susceptibility and Sustainability*, chapter 10, pages 261–286. Academic Press, New York, NY, USA, 2023. [2](#)
- [5] Zalán Borsos, Mojmír Mutný, and Andreas Krause. Coresets via bilevel optimization for continual learning and streaming. In *Advances in Neural Information Processing Systems (NeurIPS)*, 2020. [3](#)
- [6] Rania Briq, Jiangtao Wang, and Stefan Kesselheim. Data pruning in generative diffusion models. *arXiv preprint arXiv:2411.12523*, 2024. [2](#), [6](#), [7](#)
- [7] Gong Cheng, Junwei Han, and Xiaoqiang Lu. Remote sensing image scene classification: Benchmark and state of the art. *Proceedings of the IEEE*, 105(10):1865–1883, 2017. [2](#), [6](#)
- [8] Jia Deng, Wei Dong, Richard Socher, Li-Jia Li, Kai Li, and Li Fei-Fei. Imagenet: A large-scale hierarchical image database. In *Proceedings of the IEEE Conference on Computer Vision and Pattern Recognition (CVPR)*, pages 248–255, 2009. [2](#)
- [9] Runmin Dong et al. Building bridges across spatial and temporal resolutions: Reference-based super-resolution via change priors and conditional diffusion model. In *Proceedings of the IEEE/CVF Conference on Computer Vision and Pattern Recognition (CVPR)*, 2024. [1](#)
- [10] Patrick Esser, Robin Rombach, Andreas Blattmann, Dominik Lorenz, William Peebles, et al. Scaling rectified flow transformers for high-resolution image synthesis. *arXiv preprint arXiv:2403.03206*, 2024. [3](#)
- [11] Ian Goodfellow, Jean Pouget-Abadie, Mehdi Mirza, Bing Xu, David Warde-Farley, Sherjil Ozair, Aaron Courville, and Yoshua Bengio. Generative adversarial nets. In *Advances in Neural Information Processing Systems (NeurIPS)*, pages 2672–2680, 2014. [2](#)
- [12] Martin Heusel, Hubert Ramsauer, Thomas Unterthiner, Bernhard Nessler, and Sepp Hochreiter. Gans trained by a two time-scale update rule converge to a local nash equilibrium. In *Advances in Neural Information Processing Systems (NeurIPS)*, pages 6626–6637, 2017. [6](#)

[13] Jonathan Ho, Ajay Jain, and Pieter Abbeel. Denoising diffusion probabilistic models. In *Advances in Neural Information Processing Systems (NeurIPS)*, pages 6840–6851, 2020. 1

[14] Jonathan Ho, Tim Salimans, Alexey Gritsenko, William Chan, Mohammad Norouzi, and Jascha Sohl-Dickstein. Cascaded diffusion models for high fidelity image generation. In *Advances in Neural Information Processing Systems (NeurIPS)*, 2021. 3

[15] Jia-Bin Huang, Abhishek Singh, and Narendra Ahuja. Single image super-resolution from transformed self-exemplars. In *Proceedings of the IEEE Conference on Computer Vision and Pattern Recognition (CVPR)*, pages 5197–5206, 2015. 2

[16] S. Khanna, P. Liu, L. Zhou, et al. Diffusionsat: A generative foundation model for satellite imagery. *arXiv preprint arXiv:2312.03606*, 2023. 3

[17] Krishnateja Killamsetty, Durga Sivasubramanian, Ganesh Ramakrishnan, Abir De, and Rishabh Iyer. Grad-match: Gradient matching based data subset selection for efficient deep model training. In *Proceedings of the 38th International Conference on Machine Learning (ICML)*, 2021. 3

[18] Pang Wei Koh and Percy Liang. Understanding black-box predictions via influence functions. In *Proceedings of the 34th International Conference on Machine Learning (ICML)*, 2017. 3

[19] Xuecao Li, Peng Gong, Yuyu Zhou, et al. Mapping global urban boundaries from the global artificial impervious area (GAIA) data. *Scientific Data*, 7(1):168, 2020. 5

[20] Chenyang Liu et al. Text2earth: Unlocking text-driven remote sensing image generation with a global-scale dataset and a foundation model. *IEEE Geoscience and Remote Sensing Magazine*, 2025. 2, 4, 5

[21] Fan Liu, Delong Chen, Zhangqiyun Guan, Xiaocong Zhou, Jiale Zhu, Qiaolin Ye, Liyong Fu, and Jun Zhou. Remoteclip: A vision-language foundation model for remote sensing. *arXiv preprint arXiv:2306.11029*, 2023. 3

[22] Y. Liu et al. Diffusion models meet remote sensing. *arXiv preprint arXiv:2404.08926*, 2024. 3

[23] Yang Long, Yuhui Gong, Zhifeng Xiao, and Qingjie Liu. Accurate object localization in remote sensing images based on convolutional neural networks. *IEEE Transactions on Geoscience and Remote Sensing*, 55(5):2486–2498, 2017. 6

[24] Maksym Oquab, Théo Dariset, Taofik Moutakanni, Huy T. Vo, Marc Szafraniec, Vasil Khalidov, Pierre Fernandez, Daniel Haziza, Francisco Massa, Michael Rabbat, Mahmoud Assran, Nicolas Ballas, Gabriel Synnaeve, Ishan Misra, Patrick Labatut, and Armand Joulin. Dinov2: Learning robust visual features without supervision. *arXiv preprint arXiv:2304.07193*, 2023. 2, 4, 6, 7

[25] William Peebles and Saining Xie. Scalable diffusion models with transformers. *arXiv preprint arXiv:2212.09748*, 2022. 1, 3, 6

[26] G. Pleiss, T. Zhang, E. Elenberg, et al. Identifying mislabeled data using the area under the margin ranking. In *Advances in Neural Information Processing Systems (NeurIPS)*, pages 17044–17056, 2020. 2

[27] Alexander Richard, Dejan Markovic, Israel D. Gebru, Steven Krenn, Gladstone Alexander Butler, Fernando De La Torre, and Yaser Sheikh. Neural synthesis of binaural speech from mono audio. In *International Conference on Learning Representations (ICLR)*, 2021. 1

[28] Caleb Robinson, Zhicheng Hou, Konstantin Malkin, Ryan Soobitsky, Jacob Czawlytko, Jeff Mather, Scott Kadish, Jacob Shermeyer, Matthew Muckley, Ruth DeFries, et al. Large scale high-resolution land cover mapping with multi-resolution data. In *Proceedings of the IEEE/CVF Conference on Computer Vision and Pattern Recognition (CVPR)*, pages 12726–12735, 2019. 5

[29] Robin Rombach, Andreas Blattmann, Dominik Lorenz, Patrick Esser, and Björn Ommer. High-resolution image synthesis with latent diffusion models. In *Proceedings of the IEEE/CVF Conference on Computer Vision and Pattern Recognition (CVPR)*, pages 10684–10695, 2022. 3

[30] Chitwan Saharia, William Chan, Huiwen Chang, Chris Lee, Jonathan Ho, Tim Salimans, David Fleet, and Mohammad Norouzi. Palette: Image-to-image diffusion models. *ACM Transactions on Graphics (SIGGRAPH)*, 41(4), 2022. 3

[31] Chitwan Saharia, Jonathan Ho, William Chan, Tim Salimans, David J. Agrawal, Jonathan T. Barron, Ben Poole, and Mohammad Norouzi. Image super-resolution via iterative refinement. *IEEE Transactions on Pattern Analysis and Machine Intelligence*, 2022. earlier version: arXiv:2104.07636 (2021). 3

[32] Chitwan Saharia et al. Photorealistic text-to-image diffusion models with deep language understanding. In *Advances in Neural Information Processing Systems (NeurIPS)*, 2022. 3

[33] A. Sebaq and M. ElHelw. RSDiff: Remote sensing image generation from text using diffusion model. *Neural Computing and Applications*, 36(36):23103–23111, 2024. 2, 3

[34] Claude E. Shannon. A mathematical theory of communication. *Bell System Technical Journal*, 27(3):379–423, 1948. 4

[35] Yang Song, Liyue Shen, Lei Xing, and Stefano Ermon. Solving inverse problems in medical imaging with score-based generative models. *arXiv preprint arXiv:2111.08005*, 2021. 1

[36] Ben Sorscher, Robert Geirhos, Shashank Shekhar, Surya Ganguli, and Ari Morcos. Beyond neural scaling laws with simple data pruning. In *Advances in Neural Information Processing Systems (NeurIPS)*, 2022. 3

[37] Haoru Tan, Sitong Wu, Fei Du, Yukang Chen, Zhibin Wang, Fan Wang, and Xiaojuan Qi. Data pruning via moving-one-sample-out. *arXiv preprint arXiv:2310.14664*, 2023. 3

[38] Datao Tang, Xiangyong Cao, Xingsong Hou, Zhongyuan Jiang, Junmin Liu, and Deyu Meng. Crs-diff: Controllable remote sensing image generation with diffusion model. *arXiv preprint arXiv:2403.11614*, 2024. 3

[39] Aysim Toker, Marvin Eisenberger, Daniel Cremers, and Laura Leal-Taixé. Satsynth: Augmenting image-mask pairs through diffusion models for aerial semantic segmentation. In *Proceedings of the IEEE/CVF Conference on Computer Vision and Pattern Recognition (CVPR)*, 2024. 3

[40] Gui-Song Xia, Jia Hu, Fan Hu, Baoguang Shi, Xiang Bai, Yanfei Zhong, Liangpei Zhang, Xiaoqiang Lu, Han Zhang, and Xiaolin Zhu. Aid: A benchmark data set for performance

evaluation of aerial scene classification. *IEEE Transactions on Geoscience and Remote Sensing*, 55(7):3965–3981, 2017. [2](#), [6](#)

[41] Junshi Xia, Naoto Yokoya, Bruno Adriano, and Clifford Broni-Bediako. Openearthmap: A benchmark dataset for global high-resolution land cover mapping. In *Proceedings of the IEEE/CVF Winter Conference on Applications of Computer Vision (WACV)*, pages 6243–6253, 2023. [6](#)

[42] Xiaobo Xia, Jiale Liu, Jun Yu, Xu Shen, Bo Han, and Tongliang Liu. Moderate coresnet: A universal method of data selection for real-world data-efficient deep learning. In *The Eleventh International Conference on Learning Representations*, 2023. [3](#), [6](#)

[43] Yi Xiao, Qiangqiang Yuan, Kui Jiang, Jiang He, Xianyu Jin, and Liangpei Zhang. Edifssr: An efficient diffusion probabilistic model for remote sensing image super-resolution. *arXiv preprint arXiv:2310.19288*, 2023. [3](#)

[44] Kunping Yang, Gui-Song Xia, Zicheng Liu, Bo Du, Wen Yang, Marcello Pelillo, and Liangpei Zhang. Semantic change detection with asymmetric siamese networks, 2020. The SECOND dataset is released with this work. [6](#)

[45] S. Yang, P. Ye, W. Ouyang, et al. A clip-powered framework for robust and generalizable data selection. *arXiv preprint arXiv:2410.11215*, 2024. [2](#)

[46] Yi Yang and Shawn Newsam. Bag-of-visual-words and spatial extensions for land-use classification. In *Proceedings of the ACM SIGSPATIAL International Conference on Advances in Geographic Information Systems (GIS)*, pages 270–279. ACM, 2010. [6](#)

[47] Lvmin Zhang, Anyi Rao, and Maneesh Agrawala. Adding conditional control to text-to-image diffusion models. In *Proceedings of the IEEE/CVF International Conference on Computer Vision (ICCV)*, 2023. [3](#)

[48] Lei Zhang, Y. Zhao, R. Dong, et al. A<sup>2</sup>-mae: A spatial-temporal-spectral unified remote sensing pre-training method based on anchor-aware masked autoencoder. *arXiv preprint arXiv:2406.08079*, 2024. [3](#), [6](#), [7](#)

[49] Richard Zhang, Phillip Isola, Alexei A. Efros, Eli Shechtman, and Oliver Wang. The unreasonable effectiveness of deep features as a perceptual metric. In *Proceedings of the IEEE Conference on Computer Vision and Pattern Recognition (CVPR)*, pages 586–595, 2018. [6](#)

[50] Xin Zhang, Jiawei Du, Yunsong Li, Weiying Xie, and Joey Tianyi Zhou. Spanning training progress: Temporal dual-depth scoring (tdds) for enhanced dataset pruning. In *Proceedings of the IEEE/CVF Conference on Computer Vision and Pattern Recognition (CVPR)*, 2024. [3](#)

[51] Z. Zhang, T. Zhao, Y. Guo, et al. Rs5m and georsclip: A large scale vision-language dataset and a large vision-language model for remote sensing. *IEEE Transactions on Geoscience and Remote Sensing*, 2024. [2](#), [5](#)

[52] Haizhong Zheng, Rui Liu, Fan Lai, and Atul Prakash. Coverage-centric coresnet selection for high pruning rates. *arXiv preprint arXiv:2210.15809*, 2022. [3](#)